AIAA JOURNAL
Vol. 46, No. 2, February 2008

Skin-Friction Measurements and Flow Establishment Within a Long Duct at Superorbital Speeds

T. B. Silvester* and R. G. Morgan†
University of Queensland, Brisbane, Queensland 4072, Australia.

DOI: 10.2514/1.32668

The successful operation of an acceleration-compensated skin-friction transducer in test times and at total enthalpies offered by the X3 superorbital expansion tube was demonstrated. Localized measurements of skin friction and heat flux along the centerline of an inner wall of a 1-m-long rectangular diverging duct were reported. The laminar measurements were obtained in air with a freestream Mach number of 10 and stagnation enthalpy of 40 MJ/kg. Steady heat flux and skin-friction levels confirmed the establishment of quasi-steady flow periods of 350 μs along the length of the duct. Experimental results were shown to be in excellent agreement with computational fluid dynamics estimates. The measured Reynolds analogy factor was shown to be slightly higher than theoretical flat-plate predictions and computational fluid dynamics estimates, though agreement was to within experimental uncertainty. Estimates of the gas-phase and surface Damköhler numbers suggested that although the boundary layer was likely to be chemically frozen, recombination at the surface may be occurring. The experimental data and computational fluid dynamics results for a thermochemical nonequilibrium gas and catalytic and noncatalytic walls indicated that the effects of gas-phase and surface chemical reactions were negligible.

Nomenclature

C	=	calibration constant, V/Pa
C_f	=	local skin-friction coefficient
C_H	=	heat flux coefficient
C_w	=	ratio of the density-viscosity product evaluated at the wall
k_R	=	specific recombination rate coefficient, $m^6/(mol \cdot s)$
k_w	=	surface reaction rate, m/s
L	=	length of duct (1 m)
P	=	static pressure, Pa
Pr	=	Prandtl number
$\Re$	=	universal gas constant, 8.31451 $J/(mol \cdot K)$
Re_x	=	Reynolds number
Sc	=	Schmidt number
T	=	static temperature, K
t	=	time, s
u	=	velocity, m/s
V	=	voltage, V
x	=	distance from the leading edge, m
μ	=	dynamic viscosity coefficient, $Pa \cdot s$
ρ	=	density, kg/m^3
τ	=	characteristic time, s
τ_w	=	measured wall shear stress, Pa
Ω_g	=	gas-phase recombination Damköhler number
Ω_s	=	surface recombination Damköhler number
ω	=	temperature exponent

Subscripts

acc	=	acceleration component
d	=	diffusion
e	=	boundary-layer edge value
P	=	pressure component
r	=	reaction
s	=	surface reaction
sf	=	shear force component
w	=	wall value
1	=	measuring element piezoceramic
2	=	acceleration element piezoceramic
∞	=	freestream conditions (expansion-tube exit conditions)

Received 7 June 2007; revision received 19 September 2007; accepted for publication 19 September 2007.

*Postgraduate Scholar, Centre for Hypersonics; currently Senior Aerostructures Engineer, Defence Science and Technology Organisation, Brisbane, Australia; Todd.Silvester@gmail.com. Senior Member AIAA.

†Professor, Director, Centre for Hypersonics, Division of Mechanical Engineering. Associate Fellow AIAA.

I. Introduction

SKIN-FRICTION drag and the associated aerodynamic heating are critical factors for the future realization of sustained hypersonic flight. At these speeds, viscous drag and aerodynamic heating are approximately proportional to the product of the flow density (with a half-power dependency) and flight velocity squared and cubed, respectively. To explore the physical phenomena at speeds representative of actual flight requires the use of impulse facilities such as shock tubes and expansion tubes to generate the appropriate flow conditions. Experimental results have shown that viscous drag can account for up to as much as 50% of the total drag of scramjet powered vehicles [1,2]. Similar ratios have also been reported for advanced lifting bodies such as waveriders [3].

Despite the importance of skin friction to the viability and performance of slender hypersonic vehicles, its measurement in these flows has been scarce. This is primarily due to the complexities associated with measuring skin friction directly, particularly in an impulse facility environment. Consequently, the majority of investigations conducted in shock tubes or expansion tubes have relied primarily on surface heat flux measurements to explore the physical phenomena of high-enthalpy boundary layers [4–13].

Although the development of devices for the purpose of measuring skin friction began in the 1960s, success over this time has been limited [14]. In recent times, the development of skin-friction transducers for use in short-duration facilities has been reported in the literature; however, comprehensive data are rare [15–19]. The difficulties associated with measuring skin friction in impulse facilities was highlighted in the study of Kelly [20,21]. Kelly used a prototype piezoceramic transducer to measure laminar wall shear stress along a flat plate in the T4 reflected shock tunnel with flow stagnation enthalpies ranging from 2 to 12 MJ/kg. During the experiments, the raw measured signal was severely affected by high levels of acceleration and vibration and, furthermore, calibration procedures independent of the test flow were not established. During

the early 1990s, Bowersox and Schetz [22] (see also Bowersox et al. [18]) reported a skin-friction transducer capable of operating in impulse facilities with test times ranging from 400 μs to 500 ms and total stagnation enthalpies as high as 6.5 MJ/kg. The device consisted of a cantilever beam instrumented with two strain gauges mounted within an oil-filled cavity, with the floating head mounted flush with the surface. This design was later enhanced by Novean et al. [23] to increase the sensor's natural frequency and to allow measurement within a high-enthalpy flow. Preliminary tests were performed with a scramjet model in the HYPULSE expansion tube at a flow velocity of 5180 m/s and test time of 350 μs. During the tests, oil leakage from the cavity was experienced, leading to concerns of data and instrumentation contamination. Since that time, considerable work has been carried out by Schetz and his colleagues [19,24,25] at Virginia Polytechnic Institute and State University to further enhance the design, though the focus of this work is primarily transducer development.

Since the early 1990s, much work has been conducted at the University of Queensland to develop a skin-friction transducer capable of operating in the T4 reflected shock tunnel [20,21,26–28]. This work culminated with the development of an acceleration-compensated transducer [27] and provides the majority of the data published for moderate enthalpy flows. Details of the development of this novel skin-friction transducer are reported elsewhere [26].

Following earlier preliminary work [21], Goyne [26] developed an acceleration-compensated skin-friction gauge [27] for use in the T4 reflected shock tunnel. During this comprehensive investigation, Goyne measured skin friction in laminar, transitional, and turbulent constant-pressure ducted flows [29], scramjet combustors [30], and within a combusting turbulent boundary layer [31]. The majority of Goyne's experiments provided simultaneous measurements of heat flux, pressure, and skin friction along one wall of a diverging rectangular duct. By diverging the walls and modifying the leading edges, Goyne was able to mitigate a significant portion of the wave disturbances and viscous interaction effects within the duct, thereby creating a relatively constant-pressure, two-dimensional flowfield. Turbulent measurements were shown to be in good agreement with the predictions of van Driest [32] at low unit Reynolds numbers and with those of Spalding and Chi [33] at higher values. The laminar measurements were shown to be in reasonable agreement with the theory of van Driest [34], though there were only limited laminar data and experimental uncertainties were as high as $\pm 47\%$. However, to within the uncertainties, boundary-layer similarity (and hence Reynolds analogy) was shown to hold for the conditions tested. The experiments were performed at moderate-stagnation enthalpies ranging from 3 to 13 MJ/kg and, consequently, flow within the duct was chemically nonreacting for the noncombusting cases. In recent times, the work of Goyne et al. [31] has been extended by Suraweera et al. [35,36], who investigated the influence of the combustion of hydrogen in a turbulent boundary layer at total flow enthalpies ranging from 4.8 to 9.5 MJ/kg.

Although Goyne [26] demonstrated the skin-friction gauge to work well, a reliable pressure-calibration technique independent of the test flow could not be developed and there remained issues with the mounting system. These limitations have since been addressed by Silvester [28] and have significantly reduced measurement uncertainty and improved gauge operability.

This paper presents results of an expansion-tube investigation in which localized skin-friction and heat flux measurements along the centerline of an inner wall of a rectangular diverging duct were obtained. The aims of this paper are to

1) Demonstrate the successful operation of a skin-friction gauge in the reduced test times and higher total enthalpies offered by a superorbital expansion tube.

2) Obtain skin-friction data at a flow enthalpy far greater than those ever reported.

3) Demonstrate the establishment of quasi-steady flow within a long duct at superorbital speeds through surface heat flux and skin-friction measurements.

4) Investigate the applicability of Reynolds analogy at a stagnation enthalpy of 40 MJ/kg.

5) Assess the presence and influence of real gas effects on skin-friction and heat flux distributions within the duct.

II. Experimental Facility

A. X3 Superorbital Expansion Tube

The experiments were performed in the X3 superorbital expansion tube at the University of Queensland. X3 is the largest of its type and is presently capable of producing steady test flows with equivalent flight speeds up to 9.5 km/s for periods of approximately 400 μs. The X3 facility, shown schematically in Fig. 1, has a total length of 65 m, an exit diameter of 0.183 m, and a usable (uniform) test core flow diameter of 0.14 m. An idealized x–t diagram of the flow processes associated with the operation of X3 is shown in Fig. 2. The shock and acceleration tube fill pressures for the present conditions are also shown in the figure.

The operation of X3 relies on a two-stage free-piston driver [37] with a combined piston mass of 450 kg to generate a high-temperature compressed driver gas (typically, helium or a mixture of helium and argon). Upon release, the pistons are propelled along the compression tubes via a high-pressure air reservoir. The lighter primary piston (90 kg) is mechanically brought to rest at an area change (0.5- to 0.2-m diameter) midway along the compression tube [38], which allows the heavier inner piston (360 kg) to detach and further compress the driver gas ahead of it. The compression process involves transferring the piston's kinetic energy to the driver gas. When the driver gas reaches the burst pressure of the 1.6-mm mild steel primary diaphragm ($\sim$11 MPa), it ruptures. This creates a *primary* shock wave that travels along the shock tube, accelerating and heating the test gas before rupturing a *lighter* secondary diaphragm. The rupture of the secondary diaphragm causes a *secondary* shock wave to travel along the acceleration tube, while creating an unsteady expansion fan centered at the secondary diaphragm station. The formation of this unsteady expansion and associated enthalpy multiplication process [39] accelerates the test gas along the acceleration tube and into the test section at speeds in excess of 8 km/s. Further details of the theory and operation of an expansion tube are reported by Neely and Morgan [39] and Morgan [40].

For the present test conditions used (refer to Sec. II.D), the primary and secondary shock speeds were nominally 4150 and 8300 m/s, respectively. As illustrated in Fig. 2, the nominal test time commences following the passage of the starting shock (secondary shock) and the interface separating the acceleration and test gases and is terminated by the arrival of upstream expansion waves. Based on a Mirels [41] analysis for boundary-layer entrainment, the time between the shock and interface is 2 μs, which is much shorter than

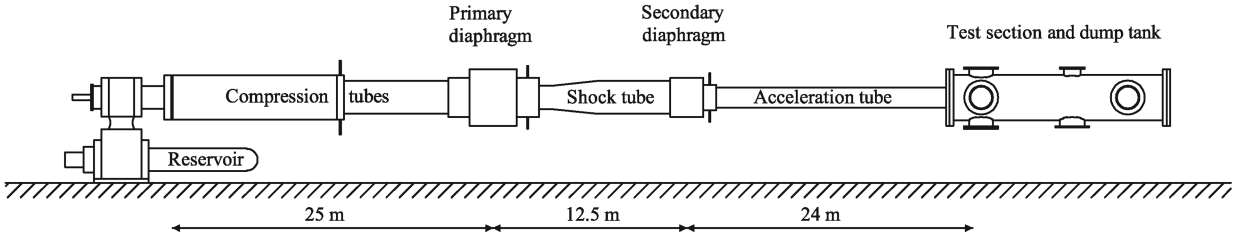

Fig. 1 Schematic of the X3 superorbital expansion tube (not to scale).

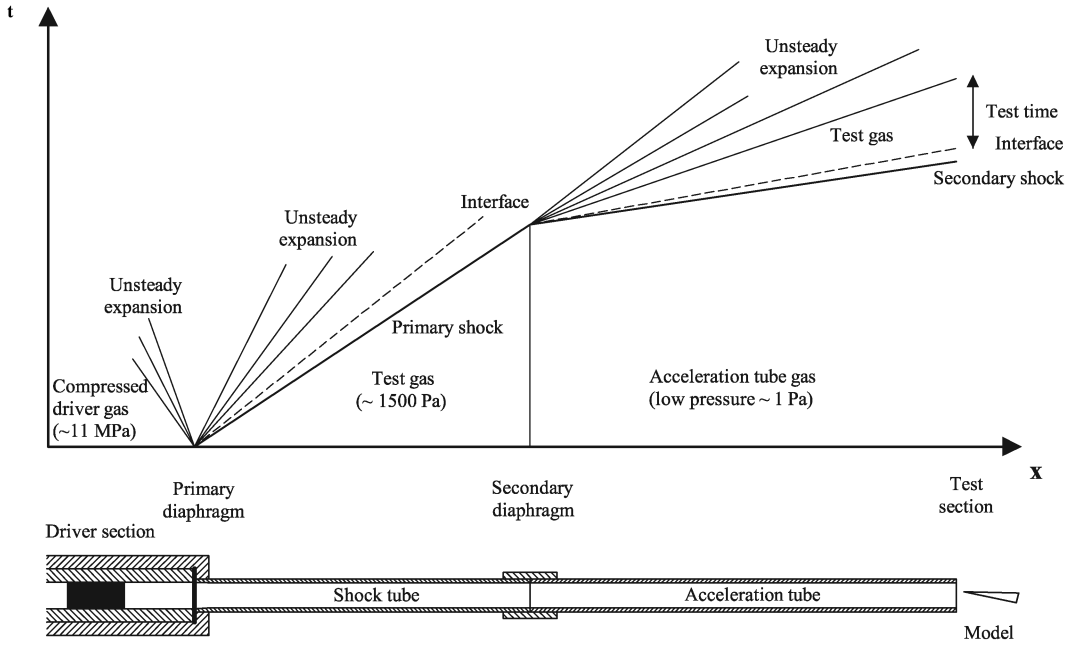

Fig. 2 Idealized $x - t$ diagram of the X3 expansion-tube facility.

the test time. Consequently, there is no need to consider the slug of acceleration gas in the flow establishment analysis, as is required in smaller expansion-tube facilities [42].

B. Test Model and Instrumentation

The test model consisted of a rectangular duct with an inlet and exit cross section of 80 × 100 mm and 100 × 100 mm, respectively. The two side walls were slightly diverged for the first 730 mm, whereas the top and bottom walls remained parallel to the flow. The overall length of the duct was 1000 mm. Following the side-wall divergence, all walls remained parallel to the centerline. The side walls were diverged linearly by 0.63 deg to delay the impact of three-dimensional corner effects. The upper wall of the duct was instrumented with heat flux gauges and skin-friction transducers along the centerline, as shown in Fig. 3. A maximum of 12 skin-friction measurement locations were possible; however, only five transducers were available, and the unused tappings were plugged with blanks. Static wall pressure measurements were also made throughout the duct during the experiments using flush-mounted PCB™ piezoceramic transducers; however, the data were unreliable. Corruption of the pressure signals was attributed to the thermal shock loads, inducing an additional response of similar magnitude to the expected pressure measurement [38]. During the test program, various coatings were applied to the sensing face to reduce the thermal effects; however, the inherent stiffness of these coatings (which altered the loading characteristics of the sensor) coupled with the low pressures caused the signals to remain unreliable. To explore this further, the thermal stressing of the sensing face (diaphragm) was analyzed analytically and experimentally [43]. The analysis revealed that the unprotected surface of a PCB transducer exposed to the flow would experience a ~3-K temperature differential through the diaphragm. Although this would induce only a small deflection of the sensing face, it is of

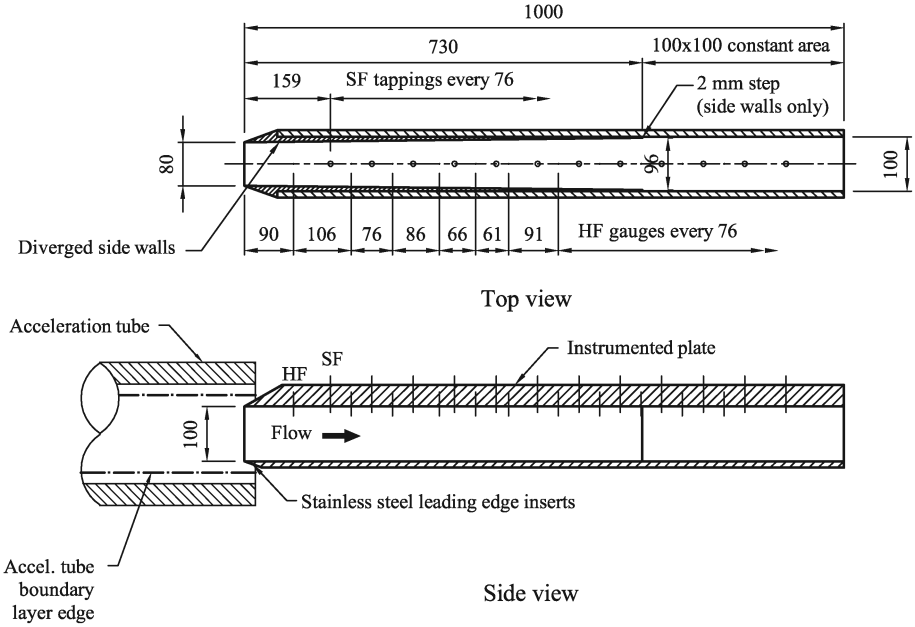

Fig. 3 Experimental duct geometry and instrumentation arrangement (dimensions in mm). HF and SF denote heat flux and skin-friction transducer locations, respectively.

sufficient magnitude to strain the crystal and induce a negative response of similar order to that experienced in this present study. Subsequently, pressure data within the duct were not considered.

The surface finish on all internal walls of the duct was manufactured to ensure that all walls were hydraulically smooth [44]. All four walls at the inlet possessed sharp leading edges and, based on the criteria of Stollery [45], the effects of finite bluntness are considered negligible. The sharp leading edges consisted of a stainless steel insert incorporated into a 20-deg bevel for the bottom and side walls and a 30-deg bevel for the top wall. A pitot pressure probe was mounted into the leading edge of the lower wall to monitor the pitot pressure during the test. The entire test duct was electrically isolated from the test section to remove conducting effects of ionization in the shock heated gas.

1. *Skin-Friction Transducer*

Direct measurements of localized skin friction were made using the acceleration-compensated skin-friction transducers developed by Goyne et al. [27] and recently enhanced by Silvester [28]. Each gauge, shown schematically in Fig. 4, is composed of a measuring element, acceleration element, and two charge amplifiers, all mounted within a brass housing. The measuring element, which is exposed to the flow, consists of a 10-mm-diam floating invar disk adhered to a piezoceramic ring. The acceleration-compensation element is shielded from the flow and is identical to the measuring element. Each piezoceramic is operated in shear mode and orientated with its direction of polarization parallel to the direction of the applied skin-friction force. This implies that the piezoceramic's sensitivity to pressure is ideally zero [26]. However, in practice, small amounts of sensitivity are observed, due to slight misalignments that occur during the construction process. Acceleration compensation is achieved by subtracting the output of the acceleration element from that of the measuring element. The measuring piezoceramic is surrounded with layers of fine brass mesh to remove heat transfer effects [27]. The skin-friction gauges have typical response times of 5 μs and a lowest natural frequency of 40 kHz.

Application of a force to the piezoceramic causes a physical deformation of the crystal, which induces a charge proportional to the applied loading. Subsequently, each gauge was calibrated for shear, acceleration [27], and pressure [28] loads in a series of separate bench tests. The resulting expression for the shear stress acting on the surface of the gauge is given by [28]

$$\tau_w = \frac{V_1 - C_{P1}P - C_{\text{acc}2}(V_2 - C_{P2}P)}{C_{\text{sf}}} \tag{1}$$

Equation (1) represents the measured shear stress compensated for vibration and pressure disturbances. However, as discussed in Section II.B, the pressure signals within the duct were negated. Subsequently, the measured shear stress signals were not compensated for pressure in this paper; instead, the measured shear stress was obtained by

$$\tau_w = \frac{V_1 - C_{\text{acc}2}V_2}{C_{\text{sf}}} \tag{2}$$

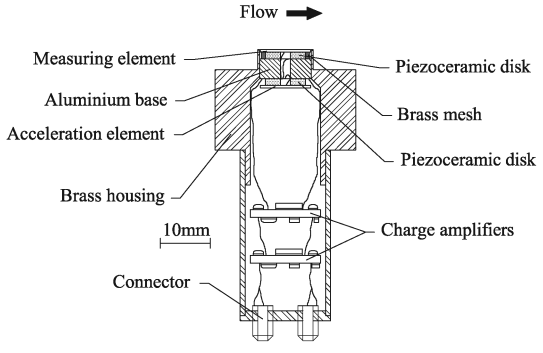

Fig. 4 Acceleration-compensated skin-friction transducer details [27].

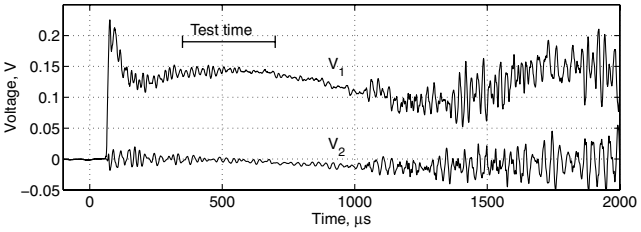

a)

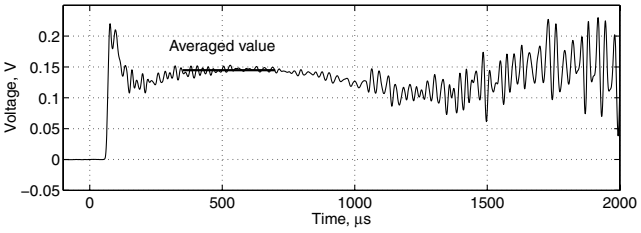

b)

Fig. 5 Skin friction gauge output in a diverging duct 40-MJ/kg test flow condition (s151): a) raw (unprocessed) output from the measuring and acceleration elements and b) compensated signal (10 μs doubled-sided moving time average).

For the test conditions considered, an uncertainty analysis demonstrates that omitting the pressure contribution to the measured shear stress introduces minimal error and increases the total uncertainty in measured shear stress from ± 7 to $\pm 9\%$ [38]. This is due to the combined effect of low static pressures (typically, less than 1.2 kPa) and moderately high levels of shear stress (typically, 150 Pa).

Figure 5 illustrates the typical raw output signals of a skin-friction gauge for the current tests. V_1 and V_2 refer to the outputs from the measuring and acceleration elements, respectively. Figure 5b shows the acceleration-compensated signal, along with the averaged value corresponding to the test interval. It is evident from the figure that a steady level of skin friction is achieved following the flow establishment for $\sim$350 μs before the test time is terminated by the arrival of the expansion waves at $\sim$700 μs. Furthermore, the results demonstrate that the transducer experienced only very low levels of acceleration during the test interval.

2. *Heat Flux Gauges*

Heat flux measurements were obtained using flush-mounted nickel-coated thin-film heat flux gauges, which were operated as electrical resistance thermometers. The gauges were manufactured in-house [46] and consisted of a nickel film, 1-mm-long $\times$ 0.3-mm-wide $\times$ 0.1-μm-thick, vacuum-deposited on a 2-mm-diam polished quartz cylinder. A 0.75-μm-thick silicon dioxide coating was also vacuum-deposited over the entire sensing face to electrically insulate the nickel from ionization in the freestream flow. During operation, the nickel film was used to monitor the time history of the surface temperature of the quartz substrate. This was then converted into a heat transfer rate following the analysis of Schultz and Jones [47]. The heat flux gauges have typical response times of 2 μs.

C. Data Acquisition

Data acquisition was performed using software and hardware developed in-house. The experimental data were digitized and recorded on three 21-channel high-speed transient data recorders, each connected to a personal computer. The software installed on each computer controlled the respective data recorder and was used to convert the raw data to an ASCII format for data postprocessing. Each data recorder had 12-bit resolution and 8 kB of data stored per channel. For the current tests, each data recorder sampled at a rate of 1 MHz and was triggered off a single pitot pressure probe

Table 1 Nominal 40 MJ/kg air freestream flow conditions

Property	Measured	Estimated
Density $\times 10 - 3$ kg/m^3	——	1.82 ± 0.32
Velocity, m/s	——	8273 ± 265
Shock velocity, m/s	7868–8320	8273 ± 265
Mach number	10.6 ± 0.7[a]	9.8 ± 0.4
Static pressure, kPa	0.8–0.95	0.92 ± 0.17
Static temperature, K	——	1419 ± 93
Total enthalpy, MJ/kg	——	39.8 ± 2.5
Pitot pressure, kPa	100–130	124 ± 9
Unit Reynolds number, m^{-1}	——	$2.81 \times 10^5 \pm 0.49 \times 10^5$
Ratio of specific heats	——	1.39 ± 0.08
Specific gas constant, J/(kg-K)	——	357 ± 38
N_2 mass fraction	——	0.74 ± 0.02
N mass fraction	——	0.05 ± 0.01
O_2 mass fraction	——	0.00 ± 0.00
O mass fraction	——	0.21 ± 0.01
NO mass fraction	——	0.00 ± 0.01

[a]Mach number deduced from the shock angle on the duct's leading-edge wedge using holographic interferometry flow visualization.

incorporated into the lower wall of the test model. This signal also allowed the synchronization of each data recorder.

D. Flow Conditions

Freestream conditions (acceleration tube exit flow conditions) were obtained from experimental measurements, numerical simulation, and theory. Finite rate chemistry computational fluid dynamics (CFD) simulation results of the facility [48] were shown to overestimate the freestream Mach number and other flow properties, due to an oversimplification of the driver and other flow processes , and are not included in this paper. Estimates of the freestream conditions shown in Table 1 were obtained from a modified JUMP analysis. JUMP [49] uses a simplified one-dimensional inviscid model of the expansion-tube flow process and is the main technique used to estimate the test conditions. JUMP incorporates a freezing velocity in which the equilibrium state of the gas is frozen at a user-specified velocity through the unsteady expansion. This velocity is iterated until the predicted pitot and static pressures match the corresponding experimental measurements. This analysis was modified to account for finite rate chemistry effects, with details reported elsewhere [38]. This analysis makes use of more experimental data (i.e., shock speeds and static and pitot pressures) than the standalone CFD simulations, enabling a better estimate of the mean freestream conditions to be obtained. Uncertainties in the freestream estimates based on a 95% confidence interval are also provided in Table 1, along with the range in measured values obtained during the experimental campaign.

Typical pitot pressure and static wall pressure traces at the exit of the acceleration tube are shown in Fig. 6, along with the local Mach number reconstructed from the pitot and static pressures using the Rayleigh pitot relation [50]. The test interval coinciding with steady levels of skin friction and heat flux is included on the plots.

All traces display a sudden increase as the shock passes over the transducer, followed by a gradual rise as the flow establishes. This is complicated further by longer rise times in the pitot pressure, due to the probe being recessed and surrounded by a protective shielding. During the test interval, the pitot and static pressures are shown to increase by approximately 15 and 20%, respectively. These result in a slight decrease in Mach number of approximately 5%. The test interval is terminated by the arrival of expansion waves. It is interesting to note that the Mach number remains relatively constant following the arrival of the expansion waves, even though the pressures decrease. The reason for this is not fully understood, but is expected to be associated with arrival and interaction of the $u - a$ and $u + a$ waves. It is likely that there is a partial cancellation effect when the reflected $u + a$ waves arrive, which causes the Mach number to remain relatively constant in regions of falling pressure. Despite this, the pressure variations during the test interval are of the order of measurement uncertainty. Furthermore, because heat flux and skin friction have a square-root dependency on pressure (through density), levels will remain relatively constant in the presence of small pressure variations, which will be shown to be the case for the present study.

III. Results

For the present conditions, the Reynolds number based on the length of the duct is 2.81×10^5 (see Table 1 and Fig. 3); consequently, natural transition is not expected to occur. Calculation of the Knudsen number as a function of the distance along a flat plate indicates that rarefaction effects should be negligible. The short test times associated with the experiments combined with the thermal mass of the duct walls ensures that the instrumented surface remains cold ($T_w = 300$ K) during a test.

A. Flow Establishment

The test interval for the experiments corresponds to the steady period in the heat flux and skin-friction time histories, which were monitored at regular intervals along the duct. Typical heat flux and skin-friction time histories at six different axial locations are shown

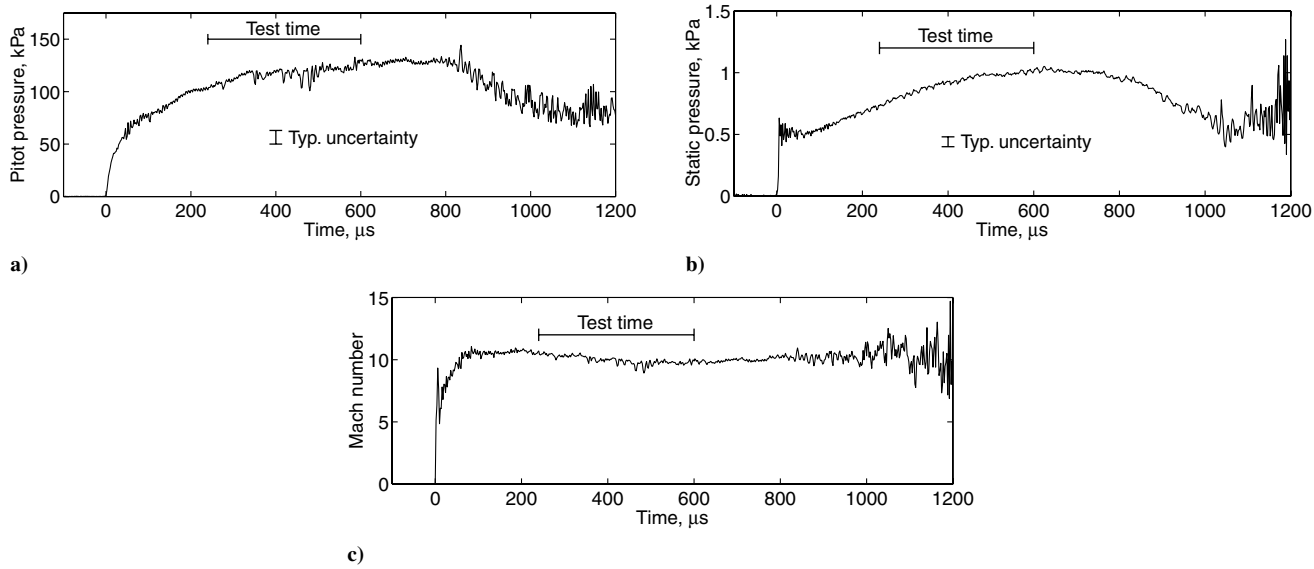

Fig. 6 Acceleration tube exit records of a) pitot pressure, b) acceleration tube static wall pressure, and c) Mach number reconstructed from pitot and static wall pressures.

in Fig. 7. The traces show a sudden increase as the shock passes over each transducer, which occurs slightly later in time at further downstream locations. This is followed by a comparatively gradual rise as the flow establishes before attaining steady values for approximately 350 μs. This steady period corresponds to the test-time interval. The test is terminated by the arrival of expansion waves, which are represented by the reduction in both heat flux and skin-friction levels.

Throughout the experiments, all time histories displayed an unsteady period following the arrival of the shock wave at each transducer. This unsteady period was observed to persist for anywhere between 230 to 300 μs. Following this interval, all time histories exhibited steady values before the arrival of the expansion waves and hence termination of the test period. The cause of this unsteady phenomenon and the fact that it exists for the same period of time at all locations is not understood in full detail, but relates to the starting process in the test facility and duct. The same phenomenon has been observed in waverider tests [51] at similar conditions, but not at lower-enthalpy conditions, though boundary-layer transition along the wall of the acceleration tube has been observed [52]. Despite this, it is concluded from the observed heat flux and skin-friction traces that quasi-steady flow establishes along the entire length of the duct following the initial unsteady phenomena. During the experiments, it was observed that the passage of this unsteady flow ranged between 2 to 2.5 duct flow lengths, following the arrival of the starting shock wave.

Heat flux traces at various axial locations along the duct are shown in Fig. 8 with a timeline marking the major occurrences throughout a typical test. The dotted horizontal lines refer to the zero level and mounting location from the leading edge for each gauge. The figure highlights that the flow establishes at each measurement location following the passage of the same slug of gas (2 to 2.5 duct flow lengths). Once the flow has established, a quasi-steady test interval of $\sim$350 μs is achieved before the test is terminated by the arrival of expansion waves.

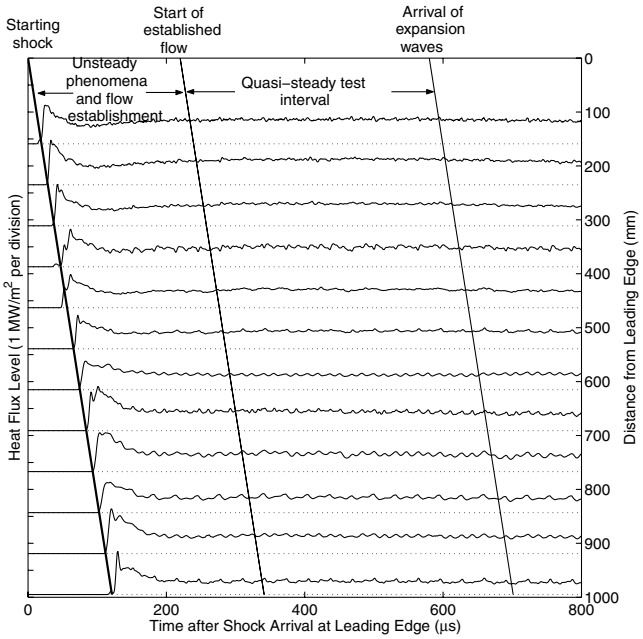

Fig. 8 Typical heat flux time histories showing the major flow occurrences throughout the duct during a test; dotted (horizontal lines) indicate the zero level and location from the leading edge for individual gauges and time zero refers to shock arrival the leading edge.

B. Centerline Axial Distributions

Centerline heat flux and skin-friction distributions averaged over the quasi-steady test interval are shown in Fig. 9 for multiple tests, along with laminar CFD estimates [38]. These data are also presented in nondimensional form in Fig. 10. However, due to the uncertainties associated with obtaining estimates of the freestream conditions, no

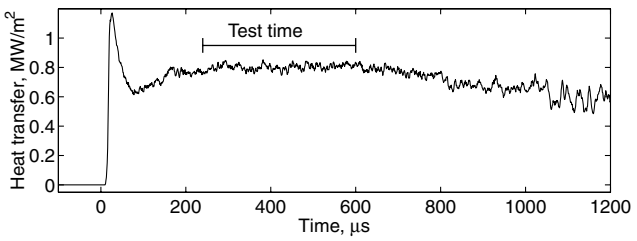

a) Location 90 mm from leading edge (s212)

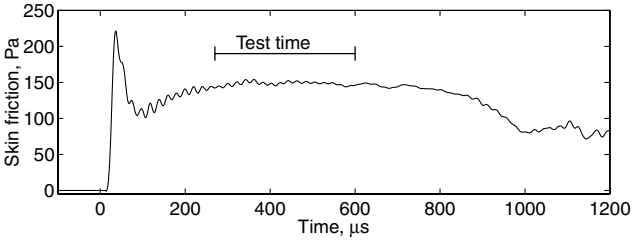

b) Location 159 mm from leading edge (s147)

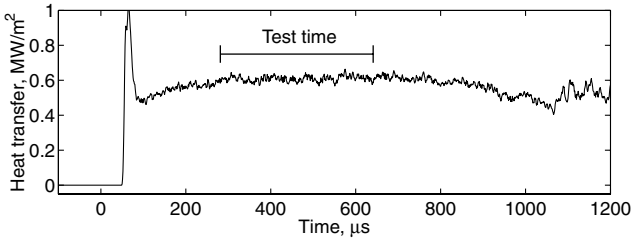

c) Location 485 mm from leading edge (s226)

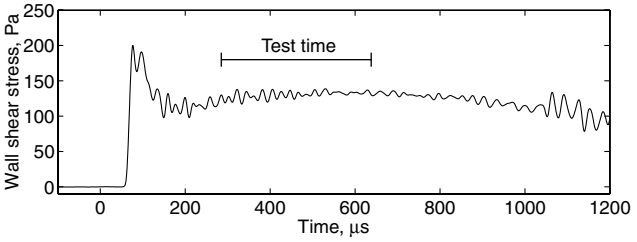

d) Location 463 mm from leading edge (s151)

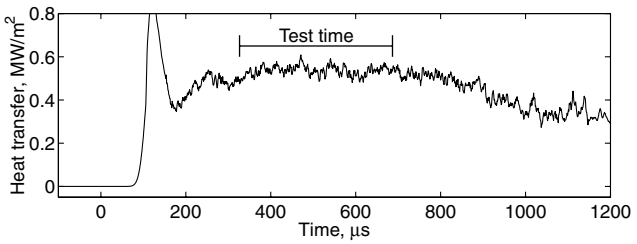

e) Location 843 mm from leading edge (s214)

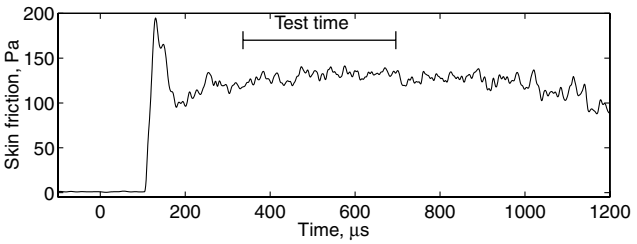

f) Location 919 mm from leading edge (s163)

Fig. 7 Typical heat flux and skin-friction traces at various streamwise locations along the inner wall of the duct (10 μs double-sided moving time averaged); time zero refers to the arrival of the shock wave at the duct's leading edge.

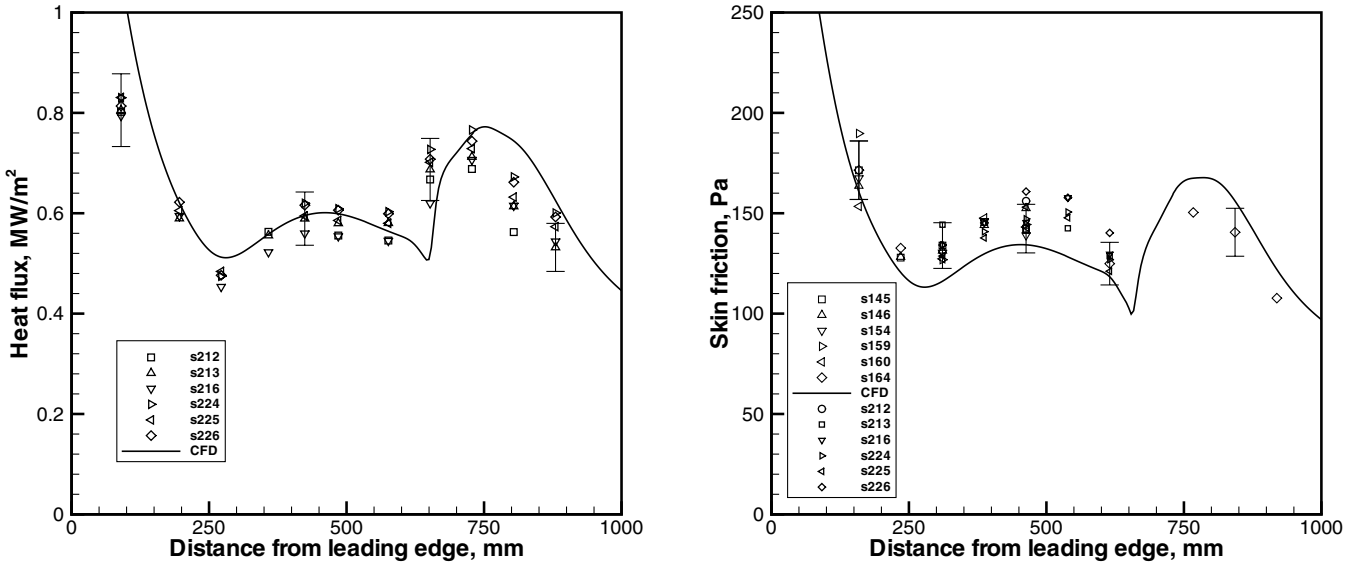

a) Heat flux b) Skin-friction

Fig. 9 Test-time-averaged centerline heat flux and skin-friction distributions.

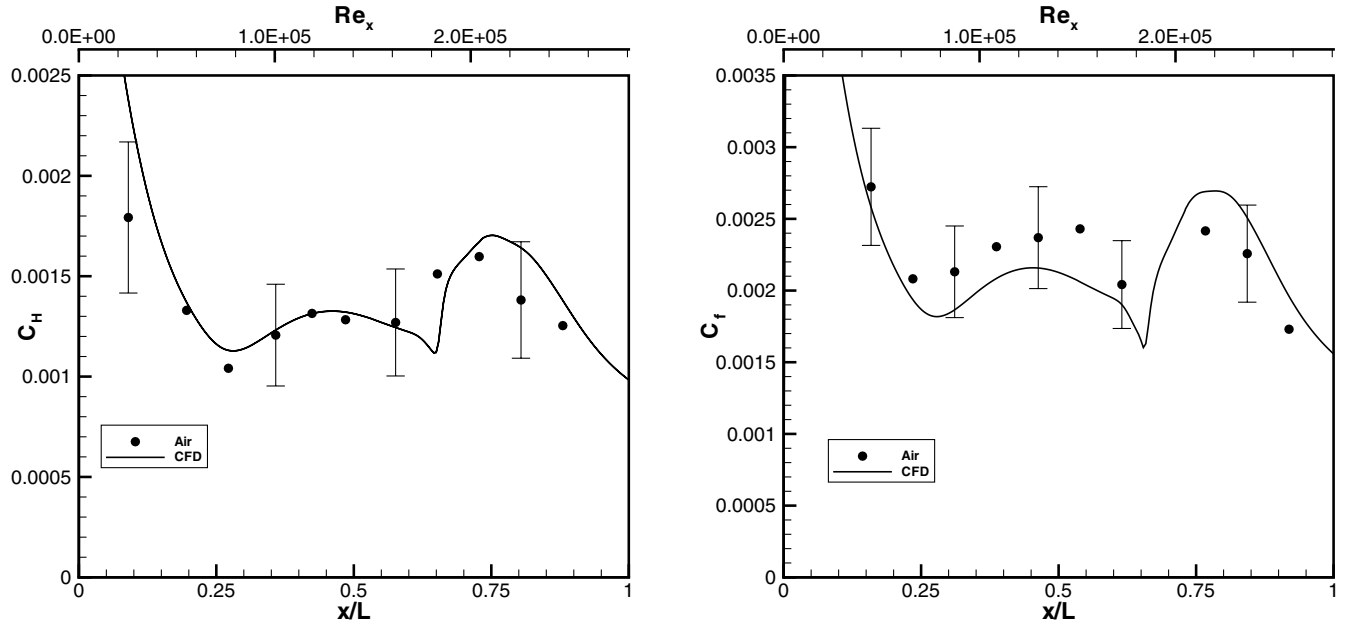

a) Heat flux b) Skin-friction

Fig. 10 Test-time-averaged centerline heat flux coefficient and skin-friction coefficient distributions; each data point represents the value averaged over multiple tests.

attempt was made to account for the variation in the freestream values from shot to shot. Instead, the data at corresponding measurement locations, as shown in Fig. 9, are averaged and nondimensionalized based on the nominal freestream conditions listed in Table 1. Although there are slight variations in the data from shot to shot, due to variations in test conditions, the measurements are shown in Fig. 9 to be repeatable to within measurement uncertainty.

The centerline distributions display a significant departure from the well-known laminar flat-plate distribution ($\propto 1/\sqrt{x}$). This departure is due to the three-dimensional viscous phenomena arising from the growth of the boundary layers along the walls of the duct and their interaction with the shock waves. Specific details of the multidimensional phenomena, including the CFD study, are the subject of a future publication and only a brief overview is given here.

The centerline distributions display the highest levels of skin friction and heat flux toward the leading edge, where the viscous interaction is strongest, before decreasing as the interaction weakens. Between $x/L = 0.25$ to 0.65, the crossflow effects emanating from the corner and passage of the side-wall shock waves cause the skin-friction and heat flux distributions to level out somewhat. At an axial location of $x/L = 0.65$, the shock wave from the lower opposing wall impinges on the upper instrumented wall and reflects slightly weakened. In the vicinity of this region, the skin friction and heat flux are increased before decaying to lower values, as represented by the "hump" in the distributions for $x/L > 0.65$.

The experimental data are shown to capture all of the aforementioned features extremely well, with experimental results in excellent agreement with CFD. Heat flux measurements at the location closest to the leading edge lie consistently below (15 to 20%) the CFD estimate, though this is only slightly greater than measurement uncertainty. The skin-friction data typically lie slightly above the CFD estimate; however, once again, agreement is to within measurement uncertainty. These results reinforce that quasi-steady flow is achieved within the duct. Furthermore, the direct

measurement of skin friction in high-enthalpy flows and reduced test times offered by a superorbital expansion tube is demonstrated.

C. Real Gas Effects

Surface heat flux levels depend on the flow chemistry within the boundary layer, which can enhance or inhibit heating. In flows with partially dissociated freestreams, such as those in a shock tube or expansion tube, the possibility exists for the recombination of atomic species to occur by gas-phase reactions within the boundary layer [11] and or by reactions at the surface in which the surface behaves as a catalyst [4,5]. When neither gas-phase or surface reactions occur, the boundary layer is chemically frozen, and the nonrecovery of the chemical enthalpy in the form of dissociated species has been shown to cause lower-than-expected heat flux values [6].

The criterion describing the likelihood of chemical recombination occurring within a boundary layer is the Damköhler number. Chung [53] proposed two separate Damköhler numbers for flow over a flat plate to describe gas-phase recombination Ω_g and recombination at the surface Ω_s. Although a flat plate was not used in this study, calculation of these Damköhler numbers is sufficient for a first-order analysis, thus providing an indication of the chemical activity within the duct. Chung defines the gas-phase Damköhler number as the ratio of characteristic boundary-layer particle diffusion time τ_d to the characteristic reaction time τ_r or, equivalently, the ratio of the reaction velocity to the flow velocity, given by

$$\Omega_g = \frac{4x}{u_e}\frac{k_{R_o}}{T_e^{(\omega+2)}}\left(\frac{P_e}{\Re}\right)^2 = \frac{\tau_d}{\tau_r} \tag{3}$$

where $k_{R_o} = 2k_R T^{\omega}$, k_R is the specific recombination rate for the reaction, the temperature exponent $\omega = 1.5$, and the universal gas constant $\Re = 8.31451\ \mathrm{J\,mol^{-1}\,K^{-1}}$. Values of $2k_R$ for reactions involving species of nitrogen and oxygen can be found in Chung [53]. For $\Omega_g \ll 1$, the diffusion rate is much greater than the reaction rate, indicating that the boundary layer is chemically frozen. Conversely, for $\Omega_g \gg 1$, the boundary layer is said to be in chemical equilibrium. If $\Omega_g \approx 1$, the boundary layer is in chemical nonequilibrium. Chung defines the surface Damköhler number as the ratio of the characteristic surface diffusion time τ_d to the characteristic surface reaction time τ_s, given by

$$\Omega_s = \frac{Sc(\rho_w k_w)}{\sqrt{[(\rho_e \mu_e)C_w u_e]/2}}\sqrt{x} = \frac{\tau_d}{\tau_s} \tag{4}$$

For $\Omega_s \to 0$, the characteristic diffusion rate is much greater than the characteristic surface reaction rate, indicating that the surface is effectively noncatalytic. As $\Omega_s \to \infty$, virtually all of the dissociated species reaching the surface will recombine, thereby increasing the heat flux to the surface. For $\Omega_s \approx 1$, the diffusion and surface reaction rates are comparable, implying that recombination at the surface could begin to influence the measured heat fluxes.

The wall reaction rate k_w in Eq. (4) is dependent on the surface material exposed to the flow. For the present study, these included mild steel (model surface) and silicon dioxide (thin-film-gauge protective coating). However, because silicon dioxide has a very low catalytic efficiency ($\sim 10^{-4}$) and is therefore highly noncatalytic, it was not considered. Although the silicon dioxide layer serves to insulate the nickel thin-film heat flux gauge from any catalytic effects, there exists the possibility that this protective layer may have been damaged or incomplete in some areas, thereby exposing the nickel strip to the dissociated test flow. Consequently, recombination of oxygen and nitrogen on both mild steel and nickel surfaces was considered. The catalytic efficiencies and wall reactions rates are given in Chung [53].

The distributions of the gas-phase Damköhler number indicate that $\Omega_g \ll 1$ over the entire length of the duct suggesting that the boundary layers are likely to be chemically frozen. The surface Damköhler number distributions indicate that $\Omega_s \sim \mathcal{O}(1)$, suggesting that recombination of atomic nitrogen may be occurring at the surface. To explore these implications further, CFD simulations of the experimental duct configuration were performed [38], which included the influence of boundary layer and wall chemistry. In the simulations, the flow chemistry was modeled three ways: 1) chemically frozen with noncatalytic walls, 2) finite rate chemistry with noncatalytic walls, and 3) finite rate chemistry with catalytic walls.

The CFD results for the *finite rate chemistry with noncatalytic walls* and the *chemically frozen with noncatalytic walls* were found to be indistinguishable from one another. This is consistent with the gas-phase Damköhler number distributions, which indicated that the boundary layers were chemically frozen. Subsequently, the only other possible mechanism for the heat flux or skin friction to be influenced by chemical reactions is if the dissociated species diffuse to the wall and recombine at the surface. Figure 11 shows these CFD

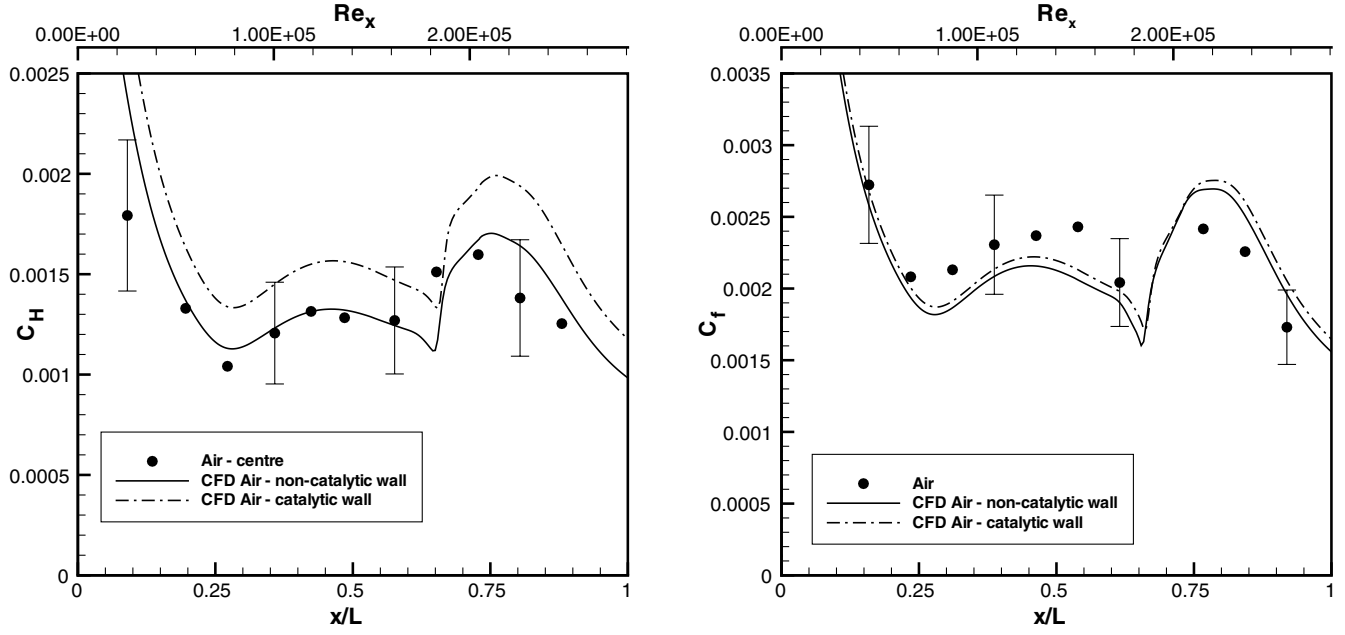

a) Heat flux b) Skin-friction

Fig. 11 Axial skin-friction and heat flux distributions for a thermally perfect gas with catalytic and noncatalytic walls.

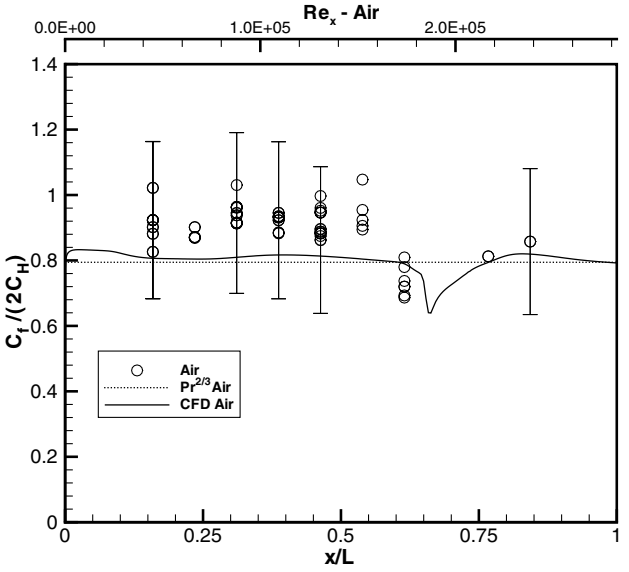

Fig. 12 Reynolds analogy factor.

results, along with the experimental centerline skin-friction and heat flux distributions. The CFD estimates show that although heat fluxes are enhanced quite dramatically due to the recovery of the chemical enthalpy, skin friction remains virtually unaffected, which is in agreement with the findings of Moss [54]. However, it is evident from Fig. 11 that any wall catalytic effects were minimal for the present conditions. Therefore, it is concluded that flow in the duct was chemically frozen and that the wall was effectively noncatalytic.

D. Laminar Reynolds Analogy

Although not strictly applicable to flows other than those over a constant-pressure flat plate, the Reynolds analogy factor is often presented for flows in scramjets [30] and ducts [29], to determine its applicability in combusting and noncombusting flows. Figure 12 shows the laminar Reynolds analogy factor for the present experiments, along with the theoretical flat-plate prediction [34] and CFD estimate. Because it was not possible to measure skin friction and heat flux at the same location simultaneously, the heat flux at each skin-friction gauge location was interpolated from the centerline values adjacent (i.e., upstream and downstream) to each skin-friction gauge. The Prandtl number for the theoretical prediction ($Pr_{\text{air}} = 0.71$) was calculated using the Groth et al. [55] high-temperature formulation.

The average measured Reynolds analogy factor for the experiments is 0.90 ± 0.20 (as a root-sum-of-squares of the systematic uncertainty and a 95% confidence interval). The measured laminar Reynolds factor is shown to lie slightly above the theoretical prediction (0.79) and CFD estimate; however, within the uncertainties, the results corroborate well with the estimate and prediction. The data are also consistent with the lower-enthalpy observations of Goyne [26], which supports Reynolds analogy in hypersonic high-enthalpy laminar boundary layers.

IV. Conclusions

This investigation successfully demonstrated, for the first time, the direct measurement of skin friction in a hypersonic flow with a stagnation enthalpy of $\sim$40 MJ/kg. Localized measurements of skin friction and heat flux along the centerline of an inner wall of a rectangular diverging duct were obtained. The experimental data confirmed the establishment of quasi-steady flow throughout the duct for a period of 350 μs. The experimental skin friction and heat flux results were shown to be repeatable to within measurement uncertainty and in excellent agreement with laminar CFD estimates. The laminar Reynolds analogy factor was calculated using the measured levels of heat flux and skin friction. Results were in good agreement with the theoretical and numerical estimates, indicating that Reynolds analogy is valid for the present conditions.

Gas-phase and surface Damköhler number distributions indicated that although the boundary layers were likely to be chemically frozen, wall catalytic effects may be present. Comparison between the CFD results and experimental data confirmed that the flow was chemically frozen and that surface catalytic effects were negligible.

Acknowledgments

The authors are thankful to Christopher Goyne for developing the skin-friction transducers and valued comments during the first author's doctorate. The authors are also appreciative of the assistance and useful discussions provided by Ray Stalker, David Mee, Michael Hayne and Ketah Jansons.

References

[1] Paull, A., Stalker, R. J., and Mee, D. J., "Experiments on Supersonic Combustion Ramjet Propulsion in a Shock Tunnel," *Journal of Fluid Mechanics*, Vol. 296, 1995, pp. 159–183. doi:10.1017/S0022112095002096

[2] Stalker, R. J., and Paull, A., "Experiments on Cruise Propulsion with a Hydrogen Scramjet," *The Aeronautical Journal*, Vol. 102, No. 1011, Jan. 1998, pp. 37–43.

[3] Anderson, J. D. Jr., *Hypersonic and High Temperature Gas Dynamics*, McGraw–Hill, New York, 1989.

[4] Simpkins, P. G., "Some Experiments in Partially Dissociated Boundary Layers," *Journal of Fluid Mechanics*, Vol. 26, No. 1, 1966, pp. 111–130. doi:10.1017/S0022112066001125

[5] Vidal, R. J., and Golian, T. C., "Heat-Transfer Measurements with a Catalytic Flat Plate in Dissociated Oxygen," *AIAA Journal*, Vol. 5, No. 9, Sept. 1967, pp. 1579–1588.

[6] East, R. A., Stalker, R. J., and Baird, J. P., "Measurements of Heat Transfer to a Flat Plate in a Dissociated High- Enthalpy Laminar Air Flow," *Journal of Fluid Mechanics*, Vol. 97, No. 4, 1980, pp. 673–699. doi:10.1017/S0022112080002753

[7] He, Y., "Boundary Layer Transition," Ph.D. Thesis, Dept. of Mechanical Engineering, Univ. of Queensland, Brisbane, Australia, 1992.

[8] Hackett, C. M., "Aerothermodynamic Heating due to Shock Wave/Laminar Boundary-Layer Interactions in High Enthalpy Hypersonic Flow," 24th Fluid Dynamics Conference, Orlando, Florida, AIAA Paper 93-3135, 6–9 July 1993.

[9] Gai, S. L., Mudford, N. R., Roberts, G. T., and Mallinson, S. G., "Effects of Catalycity and Boundary Layer Reactions on Surface Heat Flux in Hypersonic High Enthalpy Flows," *Proceedings of the 20th International Symposium on Shock Waves*, edited by B. Sturtevant, J. E. Shepherd, H. G. Hornung, Vol. 1, World Scientific, Hackensack, NJ, 1995, pp. 317–322.

[10] Neely, A. J., "Planetary Entry Aerothermodynamic Studies in a Superorbital Expansion Tube," Ph.D. Thesis, Dept. of Mechanical Engineering, Univ. of Queensland, Brisbane, Australia, 1995.

[11] Neely, A. J., and Morgan, R. G., "Heat Transfer in a Superorbital Chemically Frozen Boundary Layer," *Proceedings of the 20th International Symposium on Shock Waves*, edited by B. Sturtevant, J. E. Shepherd, H. G. Hornung, Vol. 1, World Scientific, Hackensack, NJ, 1995, pp. 251–256.

[12] Mallinson, S. G., Gai, S. L., and Mudford, N. R., "The Interaction of a Shock Wave with a Laminar Boundary Layer at a Compression Corner in High-Enthalpy Flows Including Real Gas Effects," *Journal of Fluid Mechanics*, Vol. 342, 1997, pp. 1–35. doi:10.1017/S0022112097005673

[13] Hayne, M. J., Mee, D. J., Gai, S. L., and McIntyre, T. J., "Boundary Layers on a Flat Plate at Sub- and Superorbital Speeds," *Journal of Thermophysics and Heat Transfer*, 2007 (accepted for publication).

[14] Winter, K. G., "An Outline of the Techniques Available for the Measurement of Skin Friction in Turbulent Boundary Layers," *Progress in Aerospace Sciences*, Vol. 18, 1977, pp. 1–57. doi:10.1016/0376-0421(77)90002-1

[15] Simmons, J. M., *Experimental Heat Transfer, Fluid Mechanics and Thermodynamics*, edited by M. D. Kelleher, R. K. Shah, K. R.Sreenivasan, Y. Joshi, Measurement Techniques in High Enthalpy Hypersonic Facilities, Vol. 1, Elsevier Science, New York, 1993, pp. 43–60.

[16] Jessen, C., Vetter, M., and Grönig, H., "Experimental Studies in the

Aachen Hypersonic Shock Tunnel," *Zeitschrift fur Flugwissenschaften und Weltraumforschung*, Vol. 17, No. 2, 1993, pp. 73–81.
[17] Holden, M. S., *New Trends in Instrumentation for Hypersonic Research*, edited by A. Boutier, Ground Test Facilities and Instrumentation for Aerothermal and Aero-Optical Studies of Hypersonic Interceptors, Kluwer Academic, Dordrecht, The Netherlands, 1993, pp. 65–74.
[18] Bowersox, R. D. W., Schetz, J. A., Chadwick, K., and Deiwert, S., "Technique for Direct Measurement of Skin Friction in High Enthalpy Impulsive Scramjet Flowfields," *AIAA Journal*, Vol. 33, No. 7, 1995, pp. 1286–1291.
[19] Magill, S., MacLean, M., Schetz, J. A., Kapania, R., Sang, A., and Pulliam, W., "Study of Direct-Measuring Skin-Friction Gauge with Rubber Sheet for Damping," *AIAA Journal*, Vol. 40, No. 1, 2002, pp. 50–57.
[20] Kelly, G. M., Simmons, J. M., and Paull, A., "Skin-Friction Gauge for Use in Hypervelocity Impulse Facilities," *AIAA Journal*, Vol. 30, No. 3, 1992, pp. 844–845.
[21] Kelly, G. M., "A Study of Reynolds Analogy in a Hypersonic Boundary Layer Using a New Skin Friction Gauge," Ph.D. Thesis, Dept. of Mechanical Engineering, Univ. of Queensland, Brisbane, 1994.
[22] Bowersox, R. D. W., and Schetz, J. A., "Skin Friction Gauges for High Enthalpy Impulsive Flows," AIAA Paper 93-5079, 1993.
[23] Novean, M. G., Schetz, J. A., and Bowersox, R. D. W., "Direct Measurements of Skin Friction in Complex Supersonic Flows," AIAA Paper 97-0394, 1997.
[24] Smith, T. B., Schetz, J. A., and Bui, T. T., "Development and Ground Testing of Direct Measuring Skin-Friction Gages for High Enthalpy Supersonic Flight Tests," AIAA Paper 2002-3134, 2002.
[25] MacLean, M., and Schetz, J. A., "Study of Internal Flow Effects on Direct Measurement Skin-Friction Gages," AIAA Paper 2002-0531, 2002.
[26] Goyne, C. P., "Skin Friction Measurements in High Enthalpy Flows at High Mach Number," Ph.D. Thesis, Dept. of Mechanical Engineering, Univ. of Queensland, Brisbane, Australia, 1998.
[27] Goyne, C. P., Stalker, R. J., and Paull, A., "Transducer for Direct Measurement of Skin Friction in Hypervelocity Impulse Facilities," *AIAA Journal*, Vol. 40, No. 1, Jan. 2002, pp. 42–49.
[28] Silvester, T. B., "Improvements to a Skin-Friction Transducer for Use in Impulse Facilities," *AIAA Journal* (to be published).
[29] Goyne, C. P., Stalker, R. J., and Paull, A., "Skin-Friction Measurement in High-Enthalpy Boundary Layers," *Journal of Fluid Mechanics*, Vol. 485, 2003, pp. 1–32. doi:10.1017/S0022112003003975
[30] Goyne, C. P., Stalker, R. J., and Paull, A., "Shock-Tunnel Skin-Friction Measurement in a Supersonic Combustor," *Journal of Propulsion and Power*, Vol. 15, No. 5, 1999, pp. 699–705.
[31] Goyne, C. P., Stalker, R. J., and Paull, A., "Hypervelocity Skin-Friction Reduction by Boundary-Layer Combustion of Hydrogen," *Journal of Spacecraft and Rockets*, Vol. 37, No. 6, Nov.–Dec. 2000, pp. 740–746.
[32] Van Driest, E. R., "The Problem of Aerodynamic Heating," *Aeronautical Engineering Review*, Vol. 15, No. 10, Oct. 1956, pp. 26–41.
[33] Spalding, D. B., and Chi, S. W., "The Drag of a Compressible Turbulent Boundary Layer on a Smooth Flat Plate with and Without Heat Transfer," *Journal of Fluid Mechanics*, Vol. 18, 1964, pp. 117–143. doi:10.1017/S0022112064000088
[34] Van Driest, E. R., "Investigation of Laminar Boundary Layer in Compressible Fluids Using the Crocco Method," NACA TN-2597, 1952.
[35] Suraweera, M. V., Mee, D. J., and Stalker, R. J., "Reynolds Analogy in High Enthalpy and High-Mach-Number Turbulent Flows," *AIAA Journal*, Apr. 2006, pp. 917–919.
[36] Suraweera, M. V., Mee, D. J., and Stalker, R. J., "Skin Friction Reduction in Hypersonic Turbulent Flow by Boundary Layer Combustion," AIAA Paper 2005-613, 2005.
[37] Doolan, C. J., and Morgan, R. G., "A Two-Stage Free-Piston Driver," *Shock Waves*, Vol. 9, No. 4, 1999, pp. 239–248. doi:10.1007/s001930050161
[38] Silvester, T. B., "Multidimensional Viscous Flows at Superorbital Speeds," Ph.D. Thesis, Dept. of Mechanical Engineering, Univ. of Queensland, Brisbane, Australia, 2005.
[39] Neely, A. J., and Morgan, R. G., "The Superorbital Expansion Tube Concept, experiment and Analysis," *The Aeronautical Journal*, Vol. 98, Mar. 1994, pp. 97–105.
[40] Morgan, R. G., *Handbook of Shock Waves*, edited by G. Ben-Dor, O. Igra, T. Elperin, Shock Tubes and Tunnels: Facilities, Instrumentation, and Techniques, Free-Piston Driven Expansion Tubes, Vol. 1, Academic Press, San Diego, CA, 2001, pp. 603–622.
[41] Mirels, H., "Test Time in Low-Pressure Shock Tubes," *Physics of Fluids*, Vol. 6, No. 9, Sept. 1963, pp. 1201–1214. doi:10.1063/1.1706887
[42] Hayne, M. J., "Hypervelocity Flow Over Rearward Facing Steps," Ph.D. Thesis, Dept. of Mechanical Engineering, Univ. of Queensland, Brisbane, Australia, 2004.
[43] Richards, J., "Analysis of Experimental Data of the X3 Expansion Tube," Undergraduate Thesis, Dept. of Mechanical Engineering, Univ. of Queensland, Brisbane, Australia, 2004.
[44] White, F. M., *Viscous Fluid Flow*, 2nd ed., McGraw–Hill, New York, 1991.
[45] Stollery, J. L., *Aerodynamic Problems of Hypersonic Vehicles, Viscous Interaction Effects and Re-Entry Aerothermodynamics: Theory and Experimental Results*, Lecture Series, Vol. 42, AGARD, Neuilly sur Seine, France, 1972, pp. 1–28.
[46] Hayne, M. J., "The Manufacture and Mounting of Thin Film Gauges for Heat Transfer," Dept. of Mechanical Engineering, Research Rept. 2003/20, Univ. of Queensland, Brisbane, Australia, 2003.
[47] Schultz, D. L., and Jones, T. V., "Heat-Transfer Measurements in Short-Duration Hypersonic Facilities," Advisory Group for Aerospace Research and Development, NATO, AGARDograph No. 165, 1973.
[48] Jacobs, P. A., Silvester, T. B., Morgan, R. G., Scott, M. P., Gollan, R. J., and McIntyre, T. J., "Superorbital Expansion Tube Operation: Estimates of Flow Conditions via Numerical Simulation," 43rd Aerospace Sciences Meeting, Reno, NV, AIAA Paper 2005-694, 11–13 Jan. 2005.
[49] Sutcliffe, M. A., "The Use of an Expansion Tube to Generate Carbon Dioxide Flows Applicable to Martian Atmospheric Entry Simulation," Ph.D. Thesis, Dept. of Mechanical Engineering, Univ. of Queensland, Brisbane, Australia, 1999.
[50] Owczarek, J. A., *Fundamentals of Gas Dynamics*, International Textbook, Scranton, PA, 1964.
[51] Silvester, T. B., McIntyre, T. J., and Morgan, R. G., "Superorbital Expansion Tube Tests of a Caret Waverider," *Shock Waves*, Vol. 17, Nos. 1–2, Aug. 2007, pp. 51–63. doi:10.1007/s00193-007-0100-3
[52] McGilvray, M., Jacobs, P. A., Morgan, R. G., and Ramanah, D., "Boundary Layer Transition in an Expansion Tube at a Low Enthalpy Operating Condition," AIAA Paper 2007-1328, 2007.
[53] Chung, P. M., *Advances in Heat Transfer*, edited by J. P.Hartnett, T. F. Irvine, Jr., Chemically Reacting Nonequilibrium Boundary Layers, Vol. 2, Academic Press, New York, 1965, pp. 109–270.
[54] Moss, J. N., "Reacting Viscous Shock Layer Solutions with Multicomponent Diffusion and Mass Injection," NASA TR R-411, 1974.
[55] Groth, C., Gottlieb, J., and Sullivan, P., "Numerical Investigation of High Enthalpy Temperature Effects in the UTIAS-RPI Hypersonic Impulse Tunnel," *Canadian Journal of Physics*, Vol. 69, No. 7, 1991, pp. 897–918.

N. Chokani
Associate Editor